Desalination and Water Treatment
www.deswater.com
doi: 10.1080/19443994.2015.1005686

57 (2016) 6250–6260
March

Taylor & Francis
Taylor & Francis Group

Treatment of pyridine-bearing wastewater by Nano Zero-valent iron supported on activated carbon derived from agricultural waste

Vijayalakshmi Gosu[a], Bhola Ram Gurjar[a,*], Rao Y. Surampalli[b], Tian C. Zhang[b]

[a]*Department of Civil Engineering, Indian Institute of Technology Roorkee, Roorkee 247667, Uttarakhand, India, Tel. +91 1332 285881; Fax: +91 1332 275568; emails: brgurjar@gmail.com, bholafce@iitr.ernet.in (B.R. Gurjar)*
[b]*Department of Civil Engineering, University of Nebraska–Lincoln (UNL), 205D PKI, Omaha, NE 68182-0178, USA*

Received 12 December 2013; Accepted 3 January 2015

ABSTRACT

Nano zero-valent iron particles (nZVI) supported on granular activated carbon (GAC) (nZVI/GAC) were synthesized and its feasibility was explored for the treatment of pyridine-bearing wastewater. nZVI/GAC was synthesized by the borohydride reduction method under ethanol atmosphere. The synthesized nZVI/GAC was characterized by scanning electron microscopy (SEM), X-ray diffraction, Fourier transform infrared spectroscopy, and N_2 adsorption–desorption study. Results indicated that the nZVI was well dispersed on the surface of GAC. The presence of support material apparently decreased the extent of aggregation and size of the nZVI and thus, facilitated in increasing the pyridine removal efficiency. Batch studies were carried out in order to evaluate the effect of operating parameters such as pH ($2 \le pH \le 9$), dose (m) ($5 \le m \le 15$ g/l), initial concentration (C_o) ($50 \le C_o \le 1000$ mg/l), and temperature (T) ($288 \le T \le 318$ K). At optimum condition, maximum removal of pyridine was found to be ~86% at $m = 15$ g/l, pH = 6, $C_o = 100$ mg/l, and $T = 303$ K. The degradation kinetics has been investigated, and pseudo-first-order kinetic model was found to be suitable fit for the experimental data kinetic model. The apparent activation energy (E_a) of this process was found to be ~22.46 (kJ/mol). The nZVI/GAC showed stable performance for the degradation of pyridine-bearing wastewater until five consecutive cycles.

Keywords: Nano zero-valent iron; Granular activated carbon; Pyridine; NZVI/GAC; Kinetic study

1. Introduction

Nitrogenous heterocyclic compounds are common species found in wastewater effluent, typically from pharmaceutical, paint, rubber preparation, insecticides, and petroleum industries [1]. The major nitrogenous heterocyclic compounds are pyridine, picoline, quinoline, etc. which are used in pharmaceutical industries as organic solvent for antihistamine, vitamins, and CNS stimulants. Among them, pyridine is listed as a priority organic pollutant by the United States Environmental Protection Agency. Pharmaceutical agents such as isoniazid, cetylpyridinium bromide, dermol, and cephalexin are manufactured using pyridine as catalyst [2]. The typical concentration of pyridine in wastewater produced in a multidrug intermediates product plant

*Corresponding author.

that manufactures α-picoline, 4-aminopyridine, pyridine, and other products is in the range of 20–300 mg/l [3]. The sources of pyridine from pharmaceutical industries are listed in Table 1. These compounds have received enormous attention recently because of their presence in the environment and their toxic, carcinogenic potential, and hazardous effect on the natural environment [4]. Furthermore, they possess low octanol/water partition coefficients (K_{ow}) and widely exist in the effluent of manufacturing industries [5]. Use of traditional technologies (i.e. physico-chemical and biological methods) to treat pyridine-bearing wastewater is widely reported [1–5]. The biological treatment processes are restricted to degradation under aerobic and anaerobic conditions, because of their toxicity to microbial communities. Moreover, it requires long residence time to treat refractory pollutants [6]. Other treatment processes such as incineration and advance oxidation processes require extremely high energy, capital cost, and running cost. Thermal incineration involves in incineration of organic solids into harmless end products such as CO_2, H_2O, and ash. However, the incineration process requires extremely high energy and may generate secondary pollutants [7]. In India, low volume of high strength pyridine-bearing wastewater is further concentrated in multiple-effect evaporators and incinerated in incinerators [8]. During ineffective/inefficient incineration, advance oxidation process generates toxic secondary pollutants and also generates global warming gases; however, problems may take place in the treatment system, which would force the concentrated wastewater to store, because, generally, no other alternative treatment systems exist in the plant [3]. These have achieved limited success because of their ineffectiveness against the very stable refractory and toxic compounds [9]. Therefore, it is imperative to explore/develop effective treatment technology for removal of nitrogenous heterocyclic compound such as pyridine.

During the process of selecting candidate technology for efficient treatment of pyridine wastewater, environmental nanotechnology was on the radar screen as nanotechnology has recently stimulated the growth and use of cost-effective technologies for catalytic degradation and adsorptive removal. Numerous nanocatalysts have been applied in abatement of contaminants from various environmental media. Among them, Nano zero-valent iron particles (nZVI) have a high surface area-to-volume ratio, and therefore is of a great advantage to be applied for environmental remediation [10,11]. Moreover, it exhibits unique magnetic, electrical, and chemical catalytic properties such as reductive and oxidative reactions that drive more attention in recent years. However, nZVI particles exhibit a strong tendency to agglomerate into larger aggregates due to their high surface energy and intrinsic magnetic interaction [12]. In addition, the separation and recycling of bare nZVI particles are extremely difficult. Moreover, directly using nZVI for remediation may pose certain risk to ecosystems and human health because of their potential release into the environment. An effective approach to overcome the above technical bottleneck is to fabricate hybrid nanocomposite by impregnating or coating with fine particles onto solid particles of larger size. The host materials extensively used to support nZVI are granular activated carbon (GAC) [10], silica [13], clays [11,14], alginate beads [15], and polymers [16]. GAC is particularly an attractive option partly because of its controllable pore volume and surface chemistry, as well as its excellent mechanical strength for long-term use. In addition, due to the strong attachment of organic pollutants to carbonaceous material in environmental media, GAC has shown significant application for pollution control. These properties have attracted extensive research on using GAC as immobilizing material/support.

Currently, there is a knowledge gap concerning how to make and then optimize nZVI/GAC for the degradation of pyridine in aqueous solution. The goal

Table 1
Sources of nitrogenous heterocyclic compounds in pharmaceutical industries

Sources[a]	Pollutants in effluents
Cetyl pyridine (Antiseptic)	Pyridine
Isoanizide (Tuberculosis)	Pyridine and picoline
Coramine (Respirator stimulant)	Picoline and quinoline
Demerol (Analgesic)	Pyridine and its derivatives
a-and b-Eucaine (anesthetic agents)	Pyridine and its derivatives
Cephalexin (Antibiotic)	Pyridine
Ciproflaxin	Pyridine and its derivatives

[a]Data acquired from (Mohan et al. [2]; Sims and Loughlin [4]).

of this study was to investigate the feasibility of the combined use of nZVI and GAC for treatment of wastewater contaminated by pyridine. The objectives of this paper are: introduce the synthesis of nZVI immobilized on GAC and its characterization; present the effects of various parameters on the performance of nZVI/GAC systems; and evaluate the kinetics, the reusability of nZVI/GAC, leaching of total iron, along with other issues.

2. Methods and materials

2.1. Materials and chemicals

Activated carbon derived from agriculture waste was used. Ferrous sulfate heptahydrate (SD Fine Chemicals India), sodium borohydride (SD Fine Chemicals India), pyridine (SD Fine Chemicals India), and ethanol (SD Fine Chemicals India) were used after purchases without any further treatment. All chemicals used in this study were analytical grade. Millipore water (electrical conductivity = 18 MΩ cm) made by Milli Q Water Purification System (Millipore, India) was used in this work.

2.2. Synthesis of nZVI/GAC

Synthesis of nZVI/GAC is as follows: A required quantity of $FeSO_4{\cdot}7H_2O$ was dissolved in a 4/1 (v/v) ethanol/water mixture, which was then sonicated for 10 min. Thereafter, GAC was added to the above-mentioned solution and the mixture was left in an ultrasonic shaker for 15 min in order to disperse the iron species. In the meantime, sodium borohydride solution was dissolved in Millipore water. Excess of borohydride is necessary for better growth of nanoparticles. For that reason, 20% excess BH_4^- was added. The borohydride solution was added drop wise to the iron(II) solution along with continuous stirring of the solution. Black solid particles immediately appeared after the first drop of borohydride solution. After addition of the entire borohydride solution, the mixture was left for another 10 min of stirring. Using vacuum filtration, black iron nanoparticles were separated from the liquid phase. At this stage, solid particles were washed at least three times with 25 ml ethanol to remove water content. The final step of the synthesis was to dry the synthesized nZVI/GAC in oven at 50˚C overnight. The synthesized sample was designated as 10%-nZVI/GAC. The reduction of iron ions by borohydride ions can be represented by the reaction [14].

$$Fe^{2+}_{aq} \text{ or } Fe^{2+}_{s}/GAC + 2BH^-_{4\,aq} + 6H_2O_{(l)(aq)} \rightarrow Fe^0_s + Fe^0_sGAC + 2B(OH)_{3(aq)} + 7H_{2(g)} \uparrow \quad (1)$$

In Eq. (1), Fe^{2+}_s/GAC indicates iron ions attached to GAC and Fe^0_s/GAC refers to nZVI dispersed on GAC, $Fe^0_{(s)}$ denotes nZVI.

2.3. Batch tests

For each experimental run, 100 ml solution of known pyridine concentration was taken in 250 ml conical flask containing required amount of nZVI/GAC. These flasks were agitated in a rotary shaker (Remi Instruments, Mumbai). Experiments were carried out to examine the effect of pH ($2 \le pH \le 9$), dose (m) ($5 \le m \le 15$ g/l), initial concentration (C_o) of ($50 \le C_o \le 1{,}000$ mg/l), and temperature (T) ($288 \le T \le 318$ K). The flasks were withdrawn at the end of a predetermined time (t) and the supernatant liquid was analyzed for pyridine concentration. After this period, the solution was filtered using whatman No. 42 filter paper and analyzed for the concentration of the pyridine remaining in the solution. Under these conditions, steady state was reached within 420 min. So, experiments are conducted more than 420 min. The pH was adjusted by adding 0.1 N HCl or 0.1 N NaOH solution.

2.4. Reusability

To study the reusability of synthesized nZVI/GAC, a series of repetitive experiments were performed. In each experiment, 0.2 g nZVI/GAC was added into each of the two conical flasks with 10 ml of 10 and 100 mg/l pyridine solution, respectively. After 45 min, the mixture was centrifuged and the supernatant solution was transferred. Thereafter, 10 ml portion of the fresh pyridine solution possessing the same concentration as the previous portion was added to the solid sample that remained in the conical flask. This was again shaken for 45 min afterward centrifuged, and the liquid phase was separated for the analysis. These trials were repeated such that nZVI/GAC was repeatedly exposed to five doses of 10 ml solution portions.

2.5. Kinetics analysis

Kinetics of the pyridine degradation by nZVI/GAC was performed, and results were analyzed using a first-order kinetic model:

$$-\frac{dC}{dt} = k_{obs}C = k_{SA}a_s\rho_s C = k_{SA}a_s C \quad (2)$$

$$\ln\left(C_t/C_o\right) = -k_{obs}t \quad (3)$$

$$t_{1/2} = \frac{1}{k_{obs}}\ln 2 \quad (4)$$

where C is concentration of pyridine (mg/l), k_{obs} is observed pseudo-first-order constant (1/min), k_{SA} is specific reaction rate constant (l/min m^2), a_s is specific surface area of nZVI/GAC (m^2/g), ρ_s is mass concentration of nZVI/GAC (g/l), C_o is pyridine initial concentration (mg/l), and C_t = pyridine concentration (mg/l) at time t (min).

2.6. Quality control and analytical methods

All analytical measurements are conducted in triplicate for duplicate treatments. The standard errors were calculated for analytical measurements and are depicted as error bars.

The initial and residual pyridine concentrations were determined using a UV/VIS spectrophotometer (DR500, USA). The observance of the respective solutions was measured at λ_{max} = 256 nm. The calibration plot between absorbance vs. pyridine concentration (mg/l) in aqueous solution was used to determine the concentration in the samples. The higher concentrations of pyridine samples were diluted with distilled water for the accurate determination of the pyridine concentration.

The pH of the solution was measured with pH meter (Hach, India). The total Fe concentrations were determined by the 1,10-phenanthroline spectrophotometric method.

To understand the morphology of the GAC and nZVI/GAC, a scanning electron microscope (SEM) (Quanta, Model 200 FEG, USA) was used. The samples were first gold coated with sputter coater, which provide the conductivity to the samples, and then the SEM and energy dispersive X-ray (EDX) images were taken.

The structure of the GAC and nZVI/GAC were studied with an X-ray diffractometer (XRD) (Bruker AXS, Diffractometer D8 Germany). Its analysis was done using copper as the target with nickel as the filter media, and K radiation maintained at 1.542 Å. The Goniometer speed was kept at 1° min^{-1}, with a range of the scanning angle (2θ) being 10–90°.

Textural characteristic was determined by N_2 adsorption–desorption at 77.15 K using N_2-BET analyzer (Micromeritics ASAP 2020, USA). The surface area of GAC, nZVI/GAC samples was determined using Brunauer–Emmett–Teller (BET) model in a relative pressure range of 0.05–0.30. The Barrett–Joyner–Hanlenda (BJH) method was used to calculate the pore size distribution.

Fourier transform infrared spectroscopy (FTIR) spectrometer (Thermo-Electron Corporation, USA) was employed to determine the presence of functional groups in the GAC and nZVI/GAC before and after treatment conducted at room temperature. KBr (Potassium Bromate) pellet (pressed-disk) technique was used for this purpose. The spectral range chosen was from 4,000 to 400 cm^{-1}.

3. Results and discussions

3.1. Characterization

The mesoporous structure of GAC and nZVI/GAC was investigated, and textural properties were calculated from nitrogen adsorption–desorption isotherms (Fig. 1(a) and (b) and Table 2). The isotherms of GAC and nZVI/GAC exhibited a typical type II isotherm hypothesis curve, which represents a typical mesoporous structure according to the IUPAC classification [17]. This trend implies the generation of nZVI species inside the mesoporous, being responsible for volume loss detected from adsorption isotherms. The BET surface area of the GAC and nZVI/GAC are 273 and 163 m^2/g, respectively (Table 2). The nZVI imbedded in the GAC reduce the surface area and pore volume of the GAC. The reduced pore volume was about 0.611 times lower than that of the bare GAC (0.162 cm^3/g) (Table 2). Zhang et al. [11] have observed the same trend due to nZVI dispersed on GAC. Moreover, the pore size of composite material (nZVI/GAC) was 24.2 Å, while that of bare GAC is 23.7 Å. These changes were attributed to the entry of the $NaBH_4$ solution into pores of GAC, and reduction of Fe^{2+} to form nZVI resulted in the reduction in pore volume [10].

As shown in Fig. 1(c), the nZVI/GAC showed strong peak at 42.7°, which is a characteristic reflection of zero-valent iron [18]. This also indicates that the iron is mainly in its Fe^0 state characterized by the basic reflection at 42.7° (2θ). The characteristic peaks of 42.7° and 68.25° were, respectively, assigned to the (1 1 0) and (2 0 0) plane reflections of the nZVI with a body-centered cubic (bcc) structure [19]. The other diffraction lines are arising from GAC and other associated minerals like quartz. The broad weak bands around 2θ = 26.9° together with the deviation of the baseline between 20° and 30° indicated the amorphous carbonaceous structure of organic matrix [20]. XRD

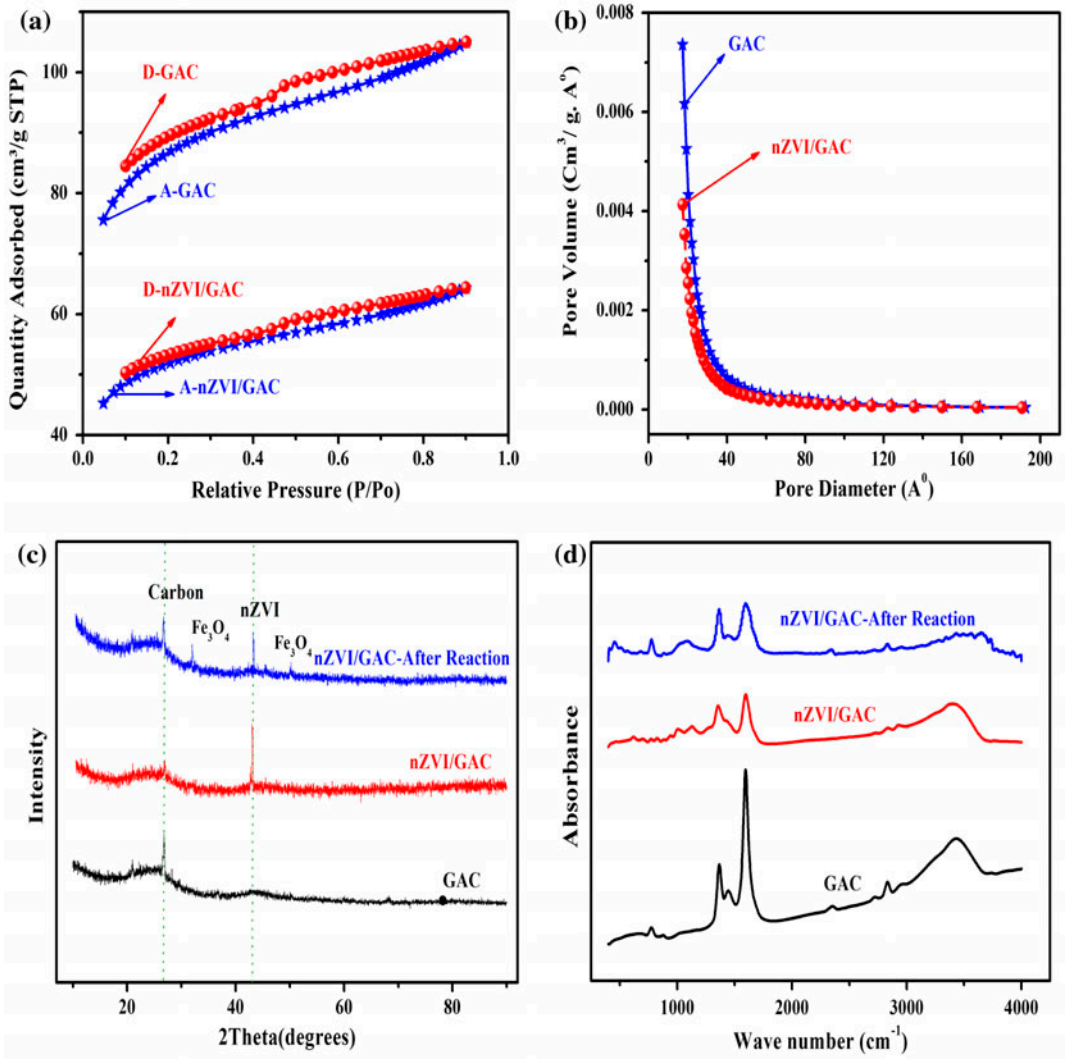

Fig. 1. (a) Nitrogen adsorption (A)–desorption (D) isotherms of GAC & nZVI/GAC, (b) pore size distributions of GAC & nZVI/GAC, (c) wide angle powder X-ray diffraction patterns of GAC, nZVI/GAC, and nZVI/GAC after reaction with pyridine, and (d) FTIR patterns of GAC, nZVI/GAC, and nZVI/GAC after reaction with pyridine.

Table 2
BET surface area, pore volume, and size of GAC and nZVI/GAC

	Surface area (m^2/g)		Pore volume (cm^3/g)		Pore size (Å)		
Material	S_{BET}[a]	Micro	BJH	Total	Micro	BJH	Average
GAC	273.025	165.7	109.4	0.162	0.08	0.078	23.7
nZVI/ GAC	163.97	99.5	65.6	0.099	0.05	0.049	24.2

[a]BET surface area.

analysis of the nZVI/GAC confirmed the existence of nZVI on the GAC.

As shown in Fig. 1(d), the broad absorbance around ~3,400 cm^{-1} is due to OH vibration and H-bonding which is a common feature indicating surface adsorption of molecular water. After immobilization of nZVI, this band shifted from 3,432 to 3,427 cm^{-1}. The Fe–O vibration was at 775 cm^{-1}, suggesting unambiguously that nZVI existed on the GAC surface [21]. In the region of 1,300–1,750 cm^{-1}, amides can be distinguished on the surface of the GAC at 1,640 and 1,450 cm^{-1} attributed to C=C, C=N, and C–N bonds [22].

From Fig. 2, it can be seen that GAC was mostly in circular shape with nonuniform micropores. After synthesis, clusters type aggregates in form of round shaped that indicate nZVI. Aggregation of nZVI is reported to be caused by the magnetic dipole–dipole interactions of the individual particles and hence reduction in their surface area [23]. The majority of the nZVI were loaded into the cracks and pores instead of surface and very significant aspect of repetitive use of

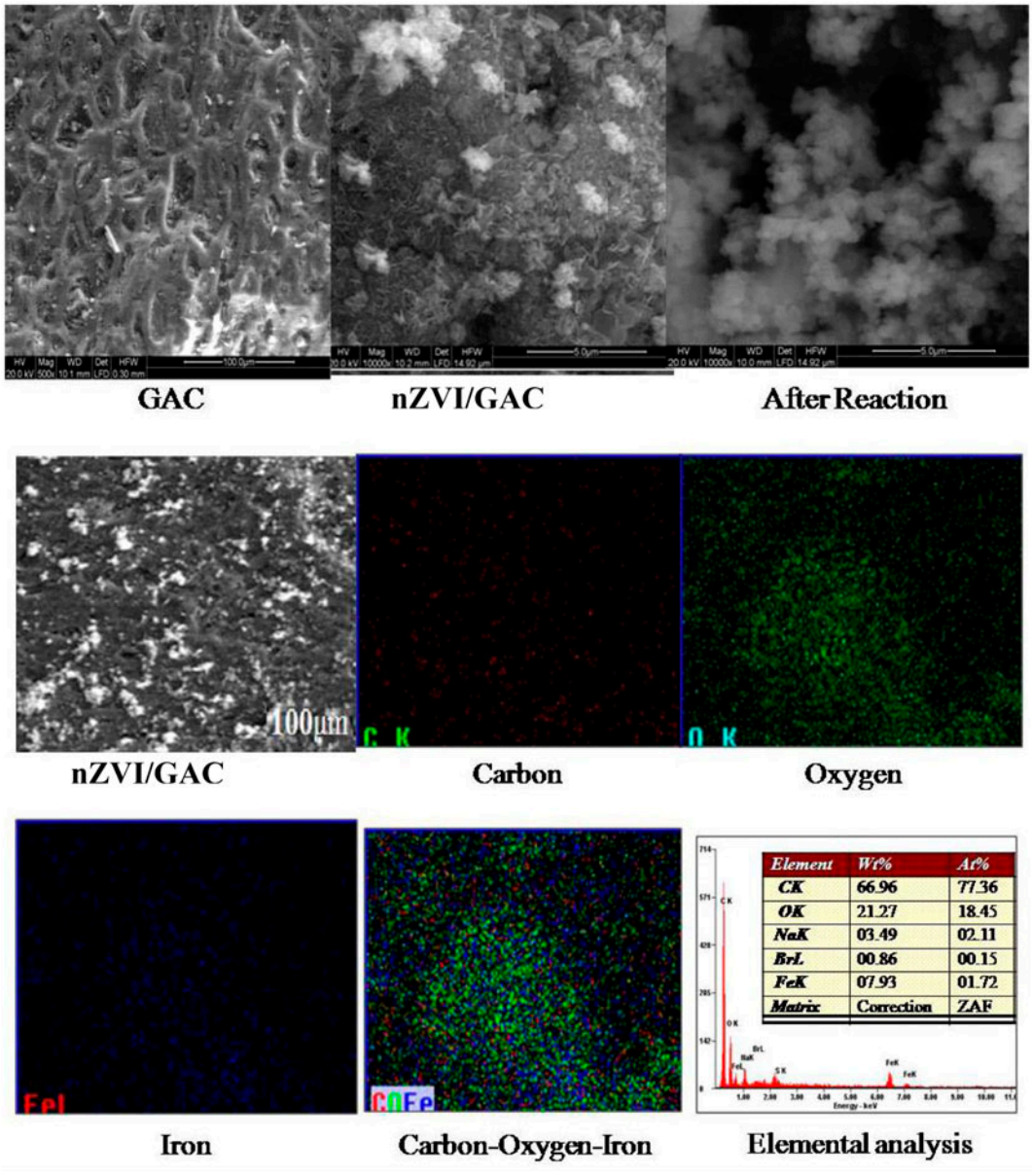

Fig. 2. SEM Images of GAC, nZVI/GAC, nZVI/GAC after reaction and EDX mapping of nZVI/GAC.

nZVI/GAC. Furthermore, Table 2 shows that GAC has 273 m^2/g surface area among that 165 m^2/g is the micropore surface area, Thus, GAC has both mesoporous and microporous surface areas.

EDX element mapping (shown in Fig. 2) showed presence of carbon, oxygen, and iron onto nZVI/GAC. These mapping images showed that the iron was well dispersed throughout the sample. Approximately, 8 wt.% iron was detected in the sample through elemental analysis.

3.2. Effect of initial pH of the solution

The pH was found to have a significant effect on the removal of pyridine by nZVI/GAC as shown in Fig. 3(a). It was observed that with an increase in pH from 2 to 6, the removal of pyridine increased gradually. A further increase in pH from 6 to 9 decreases the rate of pyridine removal. These trends may be attributed to the formations of oxide and hydroxide coatings at higher pH (>6) which hinder

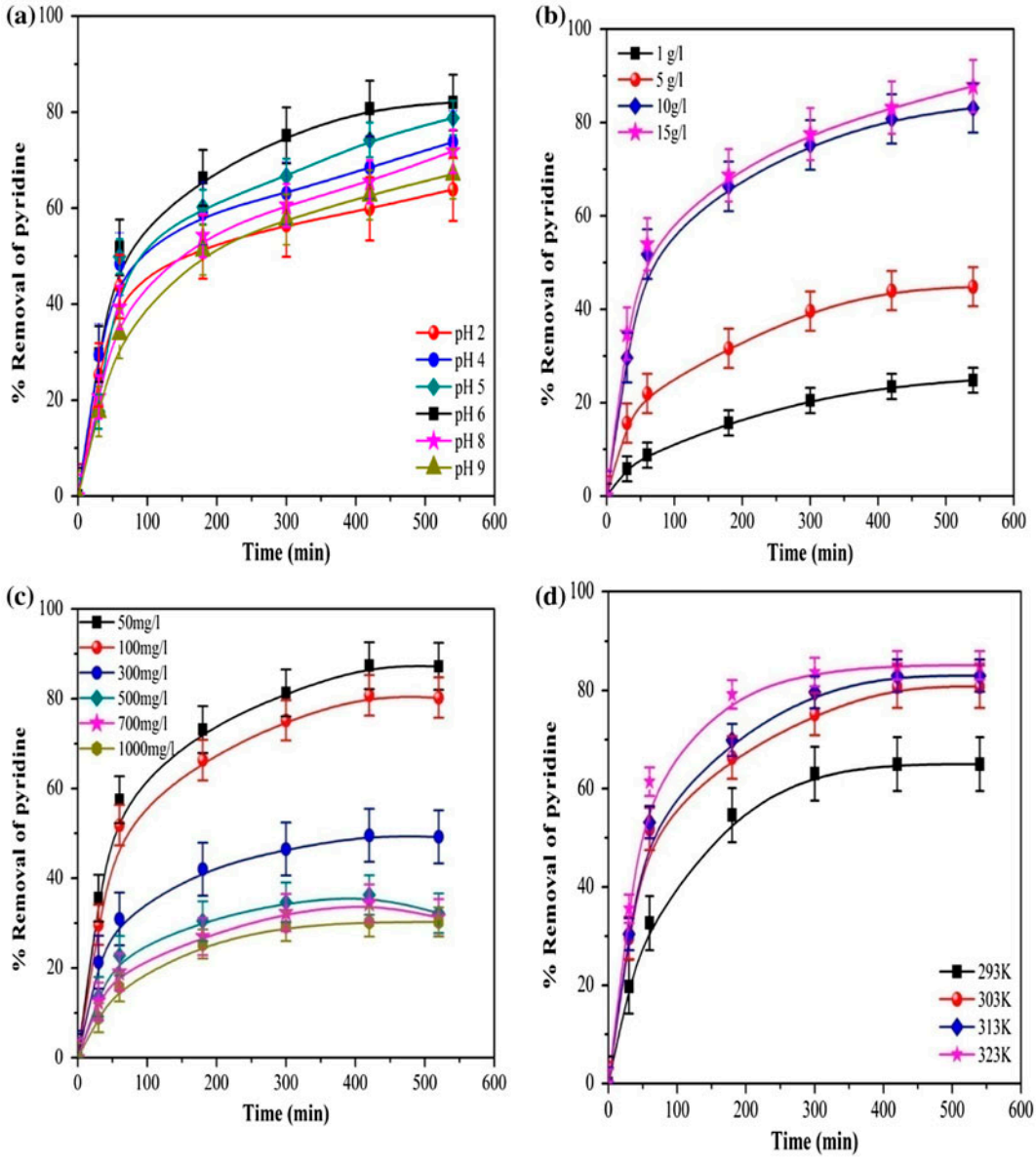

Fig. 3. (a) Effect of pH on % removal of pyridine (T = 303 K, dose = 10 g/l, C_o = 100 mg/l), (b) effect of dose (g/l) on % removal of pyridine (C_o = 100 mg/l, pH = 6, T = 303 K), (c) effect of initial concentration on % removal of pyridine (T = 303 K, dose = 15 g/l, pH = 6), and (d) effect of temperature on % removal of pyridine (C_o = 100 mg/l, dose = 15 g/l, pH = 6).

the oxidization of iron to Fe(II) ions [24]. At pH (~6), the higher removal may be ascribed to the fact that (i) the oxides on the surfaces of nanoparticles are promptly dissolved and (ii) the active sites get unlocked and iron corrosion reaction can be accelerated [25]. Moreover, pKa value of pyridine was 5.3 and it gets protonated at lower pH (i.e. <5.3) in the form of pyridium with positive charge, and deprotanated at higher pH (i.e. >5.3) that contain negative charge [8]. Furthermore, point of zero charge (PZC) of nZVI/GAC is at pH 3. When $pH > pH_{pzc,}$ nZVI/GAC surface possesses positive charge and the cations are favorably adsorbed on the surface. Whereas, $pH < pH_{pzc,}$ nZVI/GAC surface holds negative charge and the anions are preferably adsorbed on the surface. However, at the pH < 3 the surface charge of nZVI/GAC behaves as positive charge and pyridium species also possess positive charge, thus due to repulsion of same charged molecules, removal was decreased. Similarly, when pH is more than 5.3, then both pyridine species and nZVI/GAC species have negative charge, which result in predominant repulsion phenomenon. Between pH 3 and 5.3, pyridine molecules have positive charge and nZVI/GAC possess negative charge, and hence due to attraction between pyridine species and nZVI/GAC, the significant removal was observed. And also, at pH 5.3 (~6) attraction is more predominant that leads to maximum removal. Similar results were observed earlier for the adsorptive removal of pyridine by GAC, RHA [3,8].

3.3. Effect of dosage

The influence of the dose (m) (in the range of 1–20 g/l) on the removal efficiency of pyridine was studied with C_o of pyridine = 100 mg/l and T = 303 K. As shown in Fig. 3(b), the pyridine removal efficiency was found to increase with an increase of m from 1 to 10 g/l. The removal efficiency was found to be 24, 44, and 83% at m = 1, 5, and 10 g/l, respectively, at the end of the tests (540 min). This increase may be attributed to the greater number of active sites that are available at higher dosages. Lin et al. [26] reported that the heterogeneous reaction using nZVI involves five steps: (I) mass transfer of the contaminant to the nZVI surface from the bulk solution; (II) adsorption of the contaminant on the ZVI surface; (III) chemical reaction at the ZVI surface; (IV) desorption of the reaction product from the ZVI surface; and (V) mass transfer of the byproducts into the bulk solution. While the removal of pyridine by nZVI was carried out with continuous stirring, it can be speculated that step (I) may not be the control factor, whereas steps (II) and (III) probably were significant. As soon as the dose of nZVI/GAC was increased, the total particle surface areas and the active sites were increased correspondingly and thereby an increase in removal efficiencies was observed. The degradation of pyridine became almost stable at 15 g/l and above. Therefore, the dose of ~15 g/l was employed in the subsequent studies.

3.4. Effects of initial concentration

C_o of pyridine provides the necessary driving force to overcome the resistances to the mass transfer of adsorbates between the aqueous and the solid phase. The effect of C_o on removal efficiency was checked in the range of 50–1,000 mg/l at T = 303 K (Fig. 3(c)). The percentage removal decreased from 87.92% at C_o = 50 mg/l to 30.26% at C_o = 1,000 mg/l. Initially, the pyridine molecules come in contact with surface of the nZVI/GAC and reaction begins to occur. With an increase in C_o, more pyridine molecules from the aqueous solution may occupy the reaction sites or compete for reaction sites thus affects the degradation and causing decline in the reaction rate [13]. In concise, at a fixed dose, the total available sites are limited for reaction thus leading to a decrease in the percentage removal corresponding to an increase in C_o.

3.5. Effect of temperature

The results presented in Fig. 3(d) show that, with an increase in temperature, the removal efficiency increases with time. It could be due to the fact that the mobility of pyridine molecules from solution to nZVI increases at higher temperature. However, if the removal process is controlled by diffusion of pyridine species in to the pores of GAC, pyridine removal should increase with an increase in temperature because of the endothermicity of diffusion process [27,28]. An increase in temperature results in increased mobility of pyridine species and decrease in the retarding forces acting on the diffusive species. To further assess the rate-controlling steps, values of activation energy (E_a) was determined.

3.6. Determination of rate constant

To investigate the role of nZVI/GAC on pyridine degradation, the kinetic study was carried out for the treatment of pyridine-bearing wastewater as a function of time. Values of k_{obs} were obtained from the slope of the linear plot of ln (C_t/C_o). vs. t (not shown here). As shown in Table 3, the fitted curves showed a good linear relationship that confirmed the removal

Table 3
Pseudo-first-order rate constants (k_f), half life ($t_{1/2}$), and corresponding correlation coefficients (R^2) for the removal of pyridine by nZVI/GAC at different temperatures

Temperature (K)	K_{obs} (min^{-1})	R^2	Half life ($t_{1/2}$) (min)
293	0.0098	0.99	30.8
303	0.0128	0.96	23.4
313	0.0139	0.97	21.7
323	0.0248	0.99	12.1

process followed pseudo-first-order reaction kinetics. The kinetic model suggests that the reaction be limited only by the concentration of pyridine molecules [29].

The activation energy (E_a) was determined by the Arrhenius equation given as:

$$\ln k_{obs} = \ln k_o - \frac{E_a}{RT} \quad (5)$$

where k_o is frequency factor, R is molar gas constant, (E_a) is activation energy (kJ/mol), and T is the absolute temperature (K). As shown in Fig. 4(a), E_a is 22.46 kJ/mol. For diffusion-controlled reactions, E_a values are in a range of 10–15 kJ/mol [30]. In the present study, E_a value was much higher indicating the removal of pyridine was chemically controlled.

3.7. Reusability

The reusability of synthesized catalyst is a quite important factor from the practical application point of view. In this study, nZVI/GAC showed satisfactory removal efficiency until five consecutive cycles (for 10 mg/l of pyridine, up to 60%) without any regeneration (Fig. 4(b)). When the C_o was increased to 100 mg/l, a fast decline in its reactivity was observed. As illustrated by Li et al. [31], when the recycling process proceeds, the ferric oxide and hydroxide are formed on the surface of GAC and/or iron surface, blocking their active sites on the iron surface and thus, resulting in lower degradation efficiency. The amount of iron leached in the treated reaction solution was also monitored after completion of each cycle after filtration through a 0.22 μm polytetrafluoroethylene (PTFE) filter (Waters Cooperation, USA). After each cycle, total iron and Fe^{2+} concentrations were lower than 1.2 and 0.7 (not shown) mg/l, respectively. These were below permissible limit for discharge of wastewater in India [32]. The instability of the catalyst was observed visually, since after the second and third cycle a slightly brown color solution was obtained. This means that rather than dissolved iron, colloidal iron oxyhydroxide precipitates were formed, which were retained in the filtration step.

3.8. Observation of nZVI/GAC after reaction

SEM results shown in Fig. 2 represent the change in characteristics of nZVI/GAC corresponding to morphology before and after the reaction. After reacting with pyridine, the size of nZVI prominently increased and further covered with asymmetrical scaly coatings. This phenomenon could be attributed to the redox

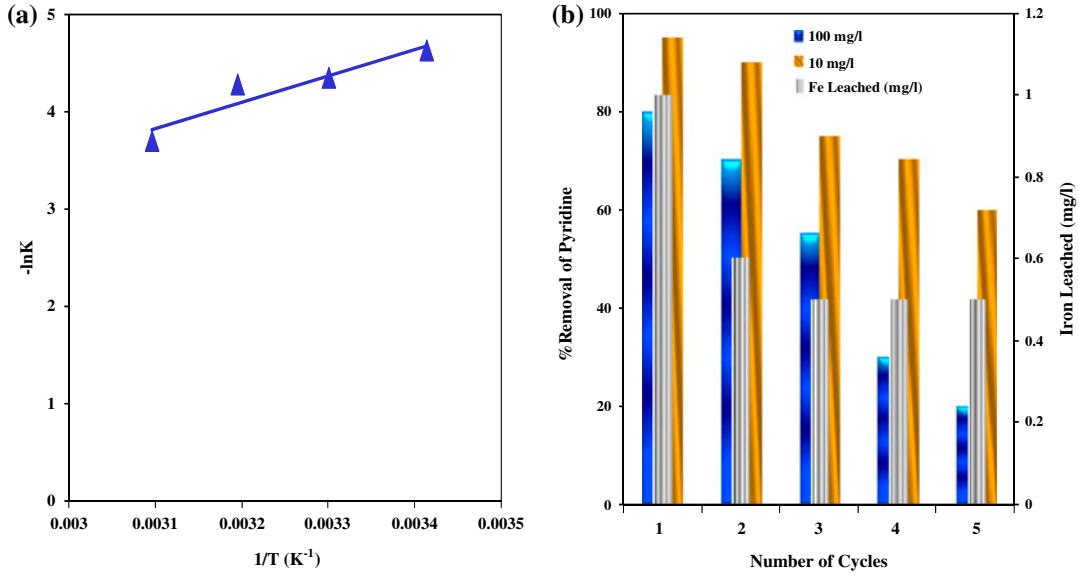

Fig. 4. (a) Determination of activation energy and (b) variation of % removal of pyridine with the number of consecutive uses.

reactions which occur during the reaction [33]. The increase in the particle aggregation is due to oxidation of nZVI in the aqueous solution that may form magnetite (Fe_3O_4), ferrous hydroxide $Fe(OH)_2$, and ferric hydroxide $Fe(OH)_3$ [34]. Therefore, it can be inferred that the aggregation of the iron was due to oxidation of nZVI in the reaction solution.

Analysis of the XRD spectrum of nZVI/GAC that had been exposed to pyridine bearing wastewater solution depicted in Fig. 1(c) reveals that magnetite (Fe_3O_4) was the major corrosive products identified based on standard Joint Committee on Powder Diffraction Standards (JCPDS) data, and the nZVI was still present. These observations are reliable with the findings of several studies, which also demonstrate the formation of iron oxides after reaction [35]. The results were supported by our XRD data, which indicated the presence of magnetite (Fe_3O_4) was formed due to the reaction(s).

FTIR spectra of nZVI/GAC before and after reaction are depicted in Fig. 1(d). After reaction, the presence of sharp bands at 3,926, 3,730, 3,646, and 3,632 cm^{-1} may be assigned to the presence of molecular water. Pyridine-containing nitrogen lone pair of electrons should overlap efficiently with localized acid sites on the nZVI surface at room temperature [36]. After reaction, a new peak band formed at 571 cm^{-1} can be ascribed to hematite phase. Similarly, goethite band was formed at 795 cm^{-1} [37]. This spectrum clearly indicates the oxidation of nZVI to form iron minerals (Fe^{2+}, Fe^{3+}).

3.9. Field applicability and unique features

Pyridine-bearing wastewater is released in substantial quantity during its manufacturing and handling operations in several industries including pharmaceutical, petroleum, petrochemical industries, and organic industries [3,38,39]. Thus, there is a huge scope to apply this technology to treat wastewater released from above stated industries. Furthermore, the unique features of this study are

(1) The agriculture waste is used in the synthesis of nanosacle zero-valent iron.
(2) Optimized the various operating parameters on the performance of nZVI/GAC systems for the degradation of pyridine.
(3) Stability of a synthesized catalyst is evaluated and one of the important aspects as to catalyst performance is considered.
(4) Observations after reaction were monitored in order to examine the transform of catalyst after reaction.

4. Conclusion

nZVI/GAC was successfully synthesized by the borohydride reduction method as revealed by XRD. EDX images showed a good dispersion of nZVI on the surface of GAC. Based on the kinetics studies, it can be inferred that the removal of pyridine can be influenced by a number of factors such as initial concentration of pyridine, the pH of solution, nZVI/GAC dose, and the reaction temperature. With an increase in the initial concentration of pyridine, a decrease in removal efficiency was observed, whereas an increase in temperature led to an increase in the removal efficiency. The maximum removal of pyridine by nZVI/GAC was found to be ~97% at a lower concentration (50 mg/l) and ~30% at a higher concentration (1,000 mg/l) using 15 g/l of nZVI/GAC. The removal of pyridine followed the pseudo-first-order reaction and the activation energy was found to be ~22.46 (kJ/mol). nZVI/GAC sustained its reactivity during five successive degradation cycles. The total amount of iron leached during the reusability tests was below 1.2 mg/l.

Acknowledgments

Authors are thankful to the Ministry of Human Resource and Development (MHRD), Government of India, for providing financial support to undertake this research work. Authors also thank the reviewers whose comments and suggestions have helped to significantly improve the manuscript. The views and opinions expressed in this article are those of the authors.

References

[1] X. Deng, C. Wei, Y. Ren, X. Chai, Isolation and identification of *Achromobacter sp.* DN-06 and evaluation of its pyridine degradation kinetics, Water Air Soil Pollut. 221 (2011) 365–375.
[2] D. Mohan, K.P. Singh, S. Sinha, D. Gosh, Removal of pyridine from aqueous solution using low cost activated carbons derived from agricultural waste materials, Carbon 42 (2004) 2409–2421.
[3] D.H. Lataye, I.M. Mishra, I.D. Mall, Removal of pyridine from aqueous solution by adsorption on bagasse fly ash, Ind. Eng. Chem. 45 (2006) 3934–3943.
[4] G.K. Sims, E.J.O. O'Loughlin, Degradation of pyridines in the environment, Crit. Rev. Env. Cont. 19 (1989) 309–340.
[5] J. Li, W. Cai, J. Cai, The characteristics and mechanisms of pyridine biodegradation by *Streptomyces sp.*, J. Hazard. Mater. 165 (2009) 950–954.
[6] G. Bertanza, C. Collivignarell, I.R. Pedrazzen, The role of chemical oxidation in combined chemical–physical and biological processes: Experience of industrial wastewater treatment, Water Sci. Technol. 44 (2001) 109–116.
[7] K. Kim, S. Ihm, Heterogeneous catalytic wet air oxidation of refractory organic pollutants in industrial

wastewaters: A review, J. Hazard. Mater. 186 (2011) 16–34.
[8] D.H. Lataye, I.M. Mishra, I.D. Mall, Pyridine sorption from aqueous solution by rice husk ash (RHA) and granular activated carbon (GAC): Parametric, kinetic, equilibrium and thermodynamic aspects, J. Hazard. Mater. 154 (2008) 858–870.
[9] N. Barrabés, J. Sá, Catalytic nitrate removal from water, past, present and future perspectives, Appl. Catal., B 104 (2011) 1–5.
[10] H.H. Tseng, J.G. Su, C. Liang, Synthesis of granular activated carbon/zero valent iron composites for simultaneous adsorption/dechlorination of trichloroethylene, J. Hazard. Mater. 192 (2011) 500–506.
[11] X. Zhang, S. Lin, Z. Chen, M. Megharaj, R. Naidu, Kaolinite-supported nanoscale zero valent iron for removal of Pb^{2+} from aqueous solution: Reactivity, characterization and mechanism, Water Res. 45 (2011) 3481–3488.
[12] F. Fu, W. Han, C. Huang, B. Tang, M. Hu, Removal of Cr(VI) from wastewater by supported nanoscale zero-valent iron on granular activated carbon, Desalin. Water Treat. 51 (2013) 2680–2686.
[13] X. Qiu, Z. Fang, B. Liang, F. Gu, Z. Jianhong, Degradation of decabromodiphenyl ether by nano zero-valent iron immobilized in mesoporous silica microspheres, J. Hazard. Mater. 71 (2011) 1091–1098.
[14] Ç. Üzüm, T. Shahwan, A.E. Eroğlu, K.R. Hallam, T.B. Scott, I. Lieberwirth, Synthesis and characterization of kaolinite-supported zero-valent iron nanoparticles and their application for the removal of aqueous Cu^{2+} and Co^{2+} ions, Appl. Clay Sci. 43 (2009) 172–181.
[15] H. Kim, H.J. Hong, J. Jung, S.H. Kim, J.W. Yang, Degradation of trichloroethylene (TCE) by nanoscale zero-valent iron (nZVI) immobilized in alginate bead, J. Hazard. Mater. 176 (2010) 1038–1043.
[16] S. Xiao, M. Shen, R. Guo, S. Wang, X. Shi, Immobilization of zerovalent iron nanoparticles into electrospun polymer nanofibers: Synthesis, characterization, and potential environmental applications, J. Phys. Chem. C 113 (2009) 18062–18068.
[17] S. Mulik, C.S. Leventis, N. Leventis, Macroporous electrically conducting carbon networks by pyrolysis of isocyanate-cross-linked resorcinol-formaldehyde aerogels, Chem. Mater. 20 (2008) 6985–6997.
[18] O. Çelebi, Ç. Üzüm, T. Shahwan, H.N. Erten, A radiotracer study of the adsorption behavior of aqueous Ba^{2+} ions on nanoparticles of zero-valent iron, J. Hazard. Mater. 148 (2007) 761–767.
[19] Z. Liu, F.S. Zhang, Nano-zerovalent iron contained porous carbons developed from waste biomass for the adsorption and dechlorination of PCBs, Bioresour. Technol. 101 (2010) 2562–2564.
[20] K. Mochidzuki, F. Soutric, K. Tadokoro, M.J. Antal, M. Tóth, B. Zelei, G. Várhegyi, Electric and physical properties of carbonized charcoals, Ind. Eng. Chem. Res. 42 (2003) 5140–5151.
[21] S. Li, P. Wu, H. Li, N. Zhu, P. Li, J. Wu, X. Wang, Z. Dang, Synthesis and characterization of organo-montmorillonite supported iron nanoparticles, Appl. Clay Sci. 50 (2010) 330–336.
[22] Z. Al-Qodah, R. Shawabkah, Production and characterization of granular activated carbon from activated sludge, Braz. J. Chem. Eng. 26 (2009) 127–136.
[23] A.R. Rahmani, H.R. Ghaffari, M.T. Samadi, A comparative study on arsenic (III) removal from aqueous solution using nano and micro sized zero-valent iron, Iran. J. Environ. Health 8 (2011) 175–180.
[24] Md. N., S. Kaneco, T. Kato, H. Katsumata, T. Suzuki, K. Ohta, Removal of thiobencarb in aqueous solution by zero valent iron, Chemosphere 70 (2008) 511–515.
[25] T.C. Zhang, Y.H. Huang, Profiling iron corrosion coating on iron grains in a zerovalent iron system under the influence of dissolved oxygen, Water Res. 40 (2006) 2311–2320.
[26] Y. Lin, C. Weng, F. Chen, Effective removal of AB24 dye by nano/micro-size zero-valent iron, Sep. Purif. Technol. 64 (2008) 26–30.
[27] V.C. Srivastava, I.D. Mall, I.M. Mishra, Multicomponent adsorption study of metal ions onto bagasse fly ash using Taguchi's design of experimental methodology, Ind. Eng. Chem. Res. 46 (2007) 5697–5706.
[28] V.C. Srivastava, I.D. Mall, I.M. Mishra, Optimization of parameters for adsorption of metal ions onto rice husk ash using Taguchi's experimental design methodology, Chem. Eng. J. 140 (2008) 136–144.
[29] S. Karthikeyan, M. Ezhil Priya, R. Boopathy, M. Velan, A.B. Mandal, G. Sekaran, Heterocatalytic fenton oxidation process for the treatment of tannery effluent: Kinetic and thermodynamic studies, Environ. Sci. Pollut. Res. 19 (2012) 1828–1840.
[30] M.J. Pilling, P.W. Seakins, Reaction Kinetics, Oxford University Press, New York, NY, 1995, p. 151.
[31] Y. Li, Y. Zhang, J. Li, G. Sheng, X. Zheng, Enhanced reduction of chlorophenols by nanoscale zerovalent iron supported on organobentonite, Chemosphere 92 (2013) 368–374.
[32] CPCB, Pollution Control acts, Rules and Notification Thereunder, Central Pollution Control Board, Govt. of India, 2001.
[33] S.M. Ponder, J.G. Darab, T.E. Mallouk, Remediation of Cr(VI) and Pb(II) aqueous solutions using supported, nanoscale zero-valent iron, Environ. Sci. Technol. 34 (2000) 2564–2569.
[34] G.N. Glavee, K.J. Klabunde, C.M. Sorensen, G.C. Hadjipanayis, Chemistry of borohydride reduction of iron(II) and iron(III) ions in aqueous and nonaqueous media. Formation of nanoscale Fe, FeB, and Fe2B powders, Inorg. Chem. 34 (1995) 28–35.
[35] W.H. Zhang, X. Quan, J.X. Wang, Z.Y. Zhang, S. Chen, Rapid and complete dechlorination of PCP in aqueous solution using Ni–Fe nanoparticles under assistance of ultrasound, Chemosphere 65 (2006) 58–64.
[36] F.M. Pan, P.C. Stair, Chemisorption of pyridine and pyrrole on iron oxide surfaces studied by XPS, Surf. Sci. 177 (1986) 1–13.
[37] Y. Xu, L. Axe, Synthesis and characterization of iron oxide-coated silica and its effect on metal adsorption, J. Colloid Interface Sci. 282 (2005) 11–19.
[38] K.V. Padoley, S.N. Mudliar, S.K. Banerjee, S.C. Deshmukh, R.A. Pandey, Fenton oxidation: A pretreatment option for improved biological treatment of pyridine and 3-cyanopyridine plant wastewater, Chem. Eng. J. 166 (2011) 1–9.
[39] V. Subbaramaiah, V.C. Srivastava, I.D. Mall, Catalytic activity of Cu/SBA-15 for peroxidation of pyridine bearing wastewater at atmospheric condition, AIChE J. 59 (2013) 2577–2586.